Surfaces and Interfaces 51 (2024) 104700

Contents lists available at ScienceDirect

Surfaces and Interfaces

journal homepage: www.sciencedirect.com/journal/surfaces-and-interfaces

A novel synthesis route with large-scale sublattice asymmetry in boron doped graphene on Ni(111)

Sumati Patil [a,*], Daniele Perilli [b], Mirco Panighel [a,1], Anu Baby [b], Cinzia Cepek [a], Giovanni Comelli [a,c], Cristiana Di Valentin [b], Cristina Africh [a]

[a] CNR - Istituto Officina dei Materiali (IOM), Laboratorio TASC, Strada Statale 14, km 163.5 Basovizza, 34149, Trieste, Italy
[b] Department of Materials Science, University of Milano-Bicocca, Via R. Cozzi 55, I-20125, Milano, Italy
[c] Department of Physics, University of Trieste, Via A. Valerio 2, 34127, Trieste, Italy

ARTICLE INFO

Keywords:
Graphene
Boron doping
Defects
Chemical vapor deposition
Scanning tunneling microscopy

ABSTRACT

One of the promising ways to functionalize graphene is incorporation of heteroatoms in carbon sp2 lattice, as it is proven to be an efficient and versatile method for controllably tuning chemistry of graphene. We present unique, contamination-free method for selectively doping graphene with B dopants, which are incorporated in layer from a reservoir created in the bulk of Ni(111) single crystal, during standard CVD growth process, leading to clean, versatile and efficient method for creating B-doped graphene. We combine experimental (STM, XPS) and theoretical (DFT, simulated STM) studies to understand structural and chemical properties of substitutional B dopants. Along with previously reported substitutional B in fcc sites, we have observed, for the first time, two more defects, namely substitutional B in top sites and interstitial B in octahedral subsurface sites. Extensive STM investigations confirm presence of low and high concentration regions of B dopants in as-prepared B-doped graphene, indicating non-uniform boron incorporation. Among two substitutional sites, no preference is observed in low-concentration B-doped regions, whereas in high B concentration regions, one of the sublattices is preferred for incorporation, along with alignment of defects. This generates an asymmetric sublattice doping in as-grown B-doped graphene, which is theoretically predicted to result in notable band gap.

1. Introduction

Since its spectacular discovery, graphene, the first free-standing 2*D* material in solid-state physics, has been thoroughly investigated and still continues to intrigue researchers with its "yet to understand" properties [1,2]. Even though pristine graphene has a unique combination of electrical [3], mechanical [4] as well as electronic [5] properties, the lack of a band gap prevents the possibility of making next-generation graphene devices for practical purposes. To overcome this limiting factor, many attempts have already been made to introduce a band gap in graphene, for example by its functionalization [6,7]. One of the most promising ways to functionalize graphene, among the multiple developed approaches, is the incorporation of heteroatoms in the carbon sp^2 lattice, as it is proven to be an efficient and versatile method for controllably tuning the chemistry of graphene [8–10]. Depending upon the heteroatom introduced, this chemically modified graphene exhibits quite interesting properties such as superconductivity, ferromagnetism [11–13] and enhanced chemical [14] and electrochemical [15,16] activity, which promote a widespread application of graphene-based materials in different technologies. Even though a variety of heteroatoms - including S, P, Se, O, Si, and I, as well as different metal atoms - have been introduced in graphene, nitrogen (N) and boron (B) have attracted most of the scientists attention because their atomic radii are similar to that of carbon (C). Specifically, N, the first heteroatom introduced in graphene, has been widely exploited for inducing n-type doping, hence representing a key element for the development of microelectronic devices [17–19]. It also can efficiently boost the catalytic performance of graphene in several electrochemical processes, especially for the oxygen reduction reaction [17]. Additionally, like other graphene functionalization strategies [20], N doping holds great potential in sensing applications [21,22]. N-doped graphene has been the focus of several studies resulting in a detailed understanding of its properties [10]. From the

* Corresponding author.
E-mail address: patil@iom.cnr.it (S. Patil).
[1] Present address: Scanning Probe Microscopy Laboratory, Department of Physics and Materials Science, University of Luxembourg, Luxembourg City L-1511, Luxembourg

https://doi.org/10.1016/j.surfin.2024.104700
Received 7 April 2024; Received in revised form 25 June 2024; Accepted 28 June 2024
Available online 29 June 2024

electronic point of view, since B has one electron less than C, it represents the other side of the coin, as it induces p-type doping in graphene [18,19]. For instance, in a theoretical study on heavily B-doped graphene (B-graphene), Dieb et al. discovered that B doping could increase the work function by 0.7 eV for concentrations above 3.1 % [23]. Also, it is observed that, as compared to N, B atoms can be embedded in graphene at higher concentrations, giving broader opportunities to tune its properties [24,25]. This makes B-graphene a unique and very attractive material from both fundamental and practical viewpoints. Recently Rao et al. investigated the B-doped topological line defect in graphene as a potential candidate to be applied as a gas-sensing device using a quantum mechanics framework for various gas molecules (CO, CO_2, NO, and NH_3) based on a combination of Density Functional Theory (DFT) and the non-equilibrium Green's function method [26].

Although the introduction of B can trigger quite interesting chemical and electrochemical activity in the graphene basal plane [27,28], B-graphene has been less well-explored experimentally: basic questions about the dopant structure, dopant distribution, and their effect on the electronic properties of graphene remain largely unanswered.

Along with the type of dopant, also the chosen underlying substrate plays a significant role in the growth process, as well as in the structure of the obtained graphene-based system. The most widely used substrates are Ni and Cu foils, but also Ru(0001), Co(0001), Ni(111), Ir(111) and Cu(111) single crystals [10,29–34]. Among these, the Ni(111) single crystal is a popular choice, as its lattice parameters are within 1.1 % those of graphene, so that, at certain growth conditions, a high-quality epitaxial layer of graphene with a (1 × 1) structure forms.

However, for B-graphene on Ni(111), a basic understanding of the structural organization from large scale to the local environment of B dopants is still not that mature, and it is the focus of the present work. We performed systematic macroscopic as well as microscopic measurements, in an effort to shed light on the local environment of incorporated B atoms in the graphene network.

Here, we present a unique, contamination-free method for the selective doping the graphene layer with B dopants -which are incorporated in the graphene layer from the reservoir created in the bulk of a Ni (111) single crystal- during the standard chemical vapor deposition (CVD) growth process, leading to a clean, versatile and efficient method of creating B-doped graphene. We have extensively investigated the synthesized B-graphene samples by means of Scanning Tunneling Microscopy (STM) to understand the local environment of the dopant. To support the observations, X-ray Photoelectron Spectroscopy (XPS) measurements as well as extensive DFT calculations, including simulated STM images, were performed. Different regions of B-graphene on Ni(111), with variable densities of B incorporation, were investigated in order to understand first the selectivity and occurrence of specific kinds of defects in the network, and, then, their effect on the electronic properties of these systems.

2. Methodology/Experimental

2.1. STM and XPS experiments

The experiments were performed in a UHV system with base pressure in the range of 1×10^{-10} mbar, equipped with a standard sample preparation facility and an Omicron variable-temperature (VT) STM operated by a R9plus controller (RHK Technology). The B-doped (see below) Ni(111) single crystal was cleaned by several subsequent cycles of Ar^+ sputtering at 1.5 kV at room temperature (RT) and annealing at 700 °C, for 10–15 min. Just after cleaning and before starting the graphene growth, sample was flash annealed at 600 °C for one minute, in order to bring B atoms towards the surface of Ni(111) single crystal. Single layer B-graphene was then grown by exposing the sample at a temperature of 580 °C to ethylene (C_2H_4, $P = 5 \times 10^{-7}$ mbar) for one hour with heating and cooling rate of 2 °C/s. In-situ low energy electron diffraction (LEED) measurements were used to confirm the growth as well as the quality of the graphene layer. In-situ high resolution STM images were then acquired in constant-current mode, with typical scanning parameters $I = 3.0$ nA, $V_{bias} = -0.2$ V, to understand the homogeneity as well as the quality of the B-graphene layer. In order to understand the repeatability and reproducibility of the as grown sample, sample preparation was repeated few times, keeping the growth parameters constant, while several locations of each sample were imaged to confirm the quality of the surface. STM images were analyzed using the Gwyddion software package with moderate noise filtering [35]. The crystallographic orientation of the images was obtained by analyzing the epitaxial structure formed by pristine graphene on the Ni(111) single crystal, as described in Ref. [36]. The sample was transferred to the XPS set up via an ultra-high vacuum suitcase. XPS measurements were then performed with a laboratory X-ray source with the base pressure in the range of 10^{-10} mbar. All spectra were collected at RT in normal emission geometry using a Mg K-alpha X-ray source (1253.6 eV) coupled with a hemispherical electron energy analyzer. Binding energies were calibrated by measuring the Fermi level. The best fit of the experimental XPS data in the B 1s region was obtained using a Shirley background and 1 Doniach-Sunjic peak, with binding energy converging to 187.29 ± 0.15 eV.

2.2. DFT calculations

DFT calculations were performed through the Quantum ESPRESSO package (QE), using a plane-wave basis set [37,38]. Ultrasoft pseudopotentials [39] were employed to describe the electron-ion interaction, treating Ni (3d, 4s), C (2s, 2p), and B (2s, 2p) as valence electrons. Based on convergence tests, energy cutoffs of 46 Ry and 326 Ry were chosen for kinetic energy and charge density expansion, respectively. For the exchange and correlation energy, we used the no-local vdW-DF2^{C09x} functional [40,41], which combines the vdW-DF2 correlation functional [40] with the C09x exchange functional [42]. This approach has been demonstrated to provide accurate predictions for adsorption geometries and electronic properties of graphene adsorbed on (111) metal surfaces, consistent with available experimental data [41]. Due to the ferromagnetic nature of Ni, spin polarization was included in all calculations. A convergence criterion of 0.026 eV/Å for forces was applied during geometry optimization (in line with previous works for graphene/Ni(111) interface [43–45]), with the total energy convergence criterion set at 10^{-6} Ry.

To model the epitaxial graphene/Ni(111) interface, we employed a (6 × 6) supercell of graphene on a (6 × 6) supercell of Ni(111), utilizing the optimized Ni(111) lattice constant of 2.46 Å, in good agreement with the experimental value of 2.4 ± 0.1 Å [46]. Consequently, we slightly adjusted the lattice constant of graphene to match the metal (lattice mismatch of 0.4 %). A vacuum layer approximately 24 Å thick in the direction perpendicular to the surface was included to prevent interactions between adjacent images. The Ni(111) surface was represented by a three-layer slab, wherein the bottom layer was fixed to bulk positions during geometry relaxation to simulate a semi-infinite solid [47]. A Monkhorst-Pack [48] k-points mesh of 3 × 3 × 1 was used for the geometry relaxation. STM simulations were performed using the Tersoff-Hamann approach [49], where the tunnelling current is proportional to the energy-integrated Local Density of States (ILDOS). Constant-current and voltage values for the STM simulations were selected to be consistent with the experimental data. Ball-and-stick models and STM images were rendered with VESTA [50] and Gwyddion [35] softwares, respectively.

3. Results and discussion

In order to obtain a single B-graphene layer on the Ni(111) substrate, a unique, contamination-free, and very clean method was developed. A Ni(111) single crystal, held at RT, was first exposed to elemental B deposition using an inhouse-built B evaporator for 30 min. The sample

was then annealed at 700 °C for 30–40 min in order to incorporate the as-deposited B in the single crystal bulk. The process of creating this B reservoir is schematically presented in Fig. 1a and 1b. The STM measurements of this substrate, presented in Fig. S1, depict a surface reconstruction which is not observed in the case of clean Ni(111) single crystal, in agreement with the theoretical indication that B incorporated in the bulk of Ni(111) single crystal tends to cause surface reconstruction [51].

Xu et al. have previously investigated the stability of on-surface B, sub-surface B, and B at the step edges of clean Ni(111) by first-principles calculations. They found that B atoms prefer the subsurface octahedral (Oct) sites over on-surface sites, and that the B binding energy increases slightly with increasing concentration of B atoms. This can be attributed to B-B interactions between the neighboring Oct sites and might suggest that subsurface B prefers to form subsurface clusters when the concentration is higher rather than distribute evenly, which eventually has a significant effect on the surface structure of the Ni(111) single crystal. The strong interaction between B atoms in neighboring Oct sites leads to the formation of B pairs. This in turn causes a surface reconstruction where one row of Ni atoms moves up by 0.27 Å, while the other moves down by 0.31 Å, so that this reconstructed surface begins to resemble a stepped surface [40]. Our STM images, presented in Fig. S1, recall this predicted stepped surface, which indicates the incorporation of B in the bulk of Ni(111) single crystal.

The B-doped Ni(111) single crystal then underwent the standard CVD graphene growth process, in which the substrate, kept at 580 °C, is exposed to ethylene (C_2H_4, $P = 5 \times 10^{-7}$ mbar) for one hour [36]. During this process the B atoms, segregating to the surface from the previously formed bulk reservoir, are expected to get trapped in the growing C network, leading to the formation of single layer of epitaxial B-graphene (Fig. 1c). The sample is then held at the growth temperature for another 10 min, to complete the growth and desorb any unreacted ethylene, and then gradually cooled down to RT at the rate of 2 °C/s (Fig. 1d).

For solid and direct evidence of the incorporation of B in the graphene network, we performed XPS measurement on the as-grown B-graphene on Ni(111). The spectra confirm the presence of B and the absence of other impurities. Fig. 2a presents the typical XPS spectrum of B 1s core level after several CVD cycles. The peak around 187.29 ± 0.15 eV can be assigned to the B atoms substitutionally incorporated into the C network, i.e. bonded to three C atoms. It has been reported that a typical B 1s spectrum recorded from B-graphene exhibits two peaks, at 188.0 eV and 187.4 eV, assigned to elemental B atoms preferably located in the Ni(111) bulk and B atoms substitutionally incorporated into the C network, respectively. Whereas, for a low B content, B 1s is reported to show only one peak at 187.3 eV [30]. Our measurements thus suggest that indeed we have B incorporation in the graphene network, at low concentration.

LEED measurements were performed to assess the long-range structure of the as-grown B-graphene on Ni(111) (Fig. S2). The diffraction pattern shows only the typical (1 × 1) graphene hexagonal pattern, indicating the absence of nickel boride on the surface. Further, extensive STM measurements were performed to understand the quality of as-grown B-graphene on Ni(111) at the atomic scale. In the regions where B concentration is sufficiently low, B atoms are expected to form single impurities, making it easier to determine the structure of B-related defects. Fig. 2b represents a typical high-resolution STM image, revealing the two most abundant defects observed in the B-graphene network. Since these defects do not appear in pristine graphene, their origin is assigned to the presence of B incorporated in different lattice sites of the sp^2 graphene network. The insets presented in Fig. 2c show in detail experimental as well as DFT simulated images of these defects along with their respective ball-and-stick models in the optimized DFT structures. These configurations were identified by replacing one of the two non-equivalent C atoms of graphene (C-top and C-fcc) with a B atom, followed by structural relaxation. The first defect is characterized by a dark triangular-shaped feature (encircled in red in Fig. 2b) centered in the fcc position. The second type appears as a brighter clover-like feature (encircled in yellow in Fig. 2b), centered in a top site, with the first fcc neighboring C atoms appearing brighter than the other C atoms of the mesh, which suggests a localized increase in the density of states. In general, such a triangular shape of impurities is a typical feature for STM images of doped graphene [29,30,52–55]. Considering their registry, we assign these two defects to fcc and top graphitic B configurations, respectively. For both these defects, this identification is confirmed by DFT calculations and corresponding simulated STM images, which nicely reproduce their appearance. While substitutional B at fcc (B-fcc) was already reported [30], to the best of our knowledge this is the first time B at top (B-top) defects are observed in B-graphene on Ni (111) single crystal.

Previous studies report that, in the case of low B doping levels, B atoms only occupy the fcc substitutional sites of graphene, as this configuration is predicted to be the most energetically favored [24]. On the other hand, our observation, deducted from different STM images acquired at several locations of B-graphene, demonstrates the presence of B in both the graphene sublattices, although with a slight preference for B atoms to occupy fcc sites.

Along with these two peculiar defects, there is one which has been observed a few times and can be correlated to the presence of a B atom in the subsurface of Ni(111) due to its appearance like a protrusion on the surface. Fig. 3 represents a region where this defect is present (encircled in yellow), along with the more abundant B-fcc (dark triangular-shaped feature). Typically, the equilibrium sites for B atoms in the Ni(111) subsurface are the tetrahedral and Oct sites, with the latter, where the B atom is surrounded by three surface Ni atoms and three subsurface Ni atoms, predicted to be the most favorable [56]. To verify this hypothesis, we considered various models where an additional B atom was introduced into different interstitial sites of Ni(111). After atomic relaxation, we found that the most stable configuration is with the B atom at the Oct site. As shown in Fig. 3, the simulated STM image closely resembles the experimentally observed appearance of this defect, with a bright spot corresponding to the C atom positioned directly above the subsurface B atom. To the best of our knowledge, this is the first experimental observation of the presence of B in the subsurface of Ni(111) single crystal. The observation of this type of defect supports the presence of a B reservoir in the Ni(111) bulk.

Besides the above discussed main defects, we have observed a small fraction of few other defects with threefold symmetry, presented in

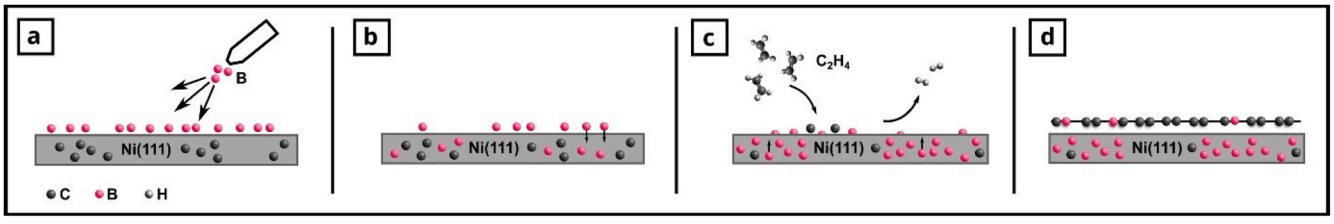

Fig. 1. Schematic illustration representing: (a) controlled B deposition on Ni(111) by a B evaporator; (b) followed by annealing the substrate to incorporate B in the bulk of the crystal; (c) subsequent exposure to ethylene in UHV conditions; (d) formation of single layer B-graphene.

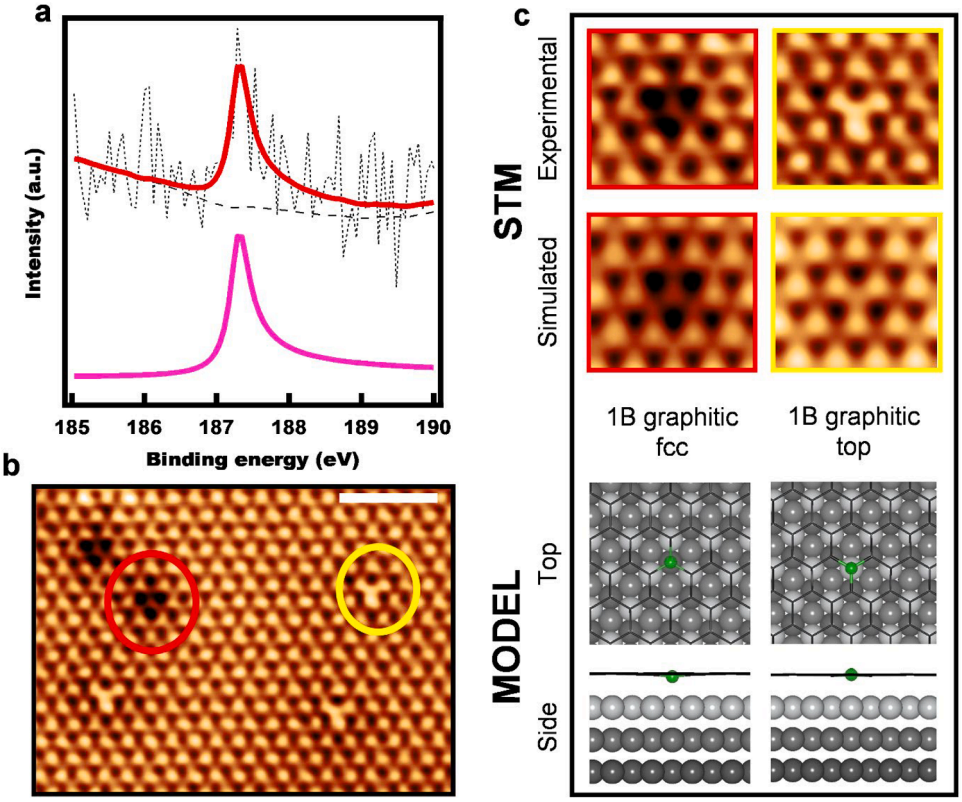

Fig. 2. (a) XPS spectrum of the B 1s core level acquired in the presence of B-graphene, along with the corresponding peak fitting analysis (Pink curve). The black dotted line corresponds to the raw data, whereas the red colored line represents the fitting. (b) STM images depicting different defects present on the surface and assigned to substitutional B. Scale bar 1.5 nm. (c) The two most abundant types of defects (namely B-fcc, B- top) along with their STM images (experimental and simulated) and ball-and-stick models are visualized. Experimental parameters: $I = 3.0$ nA, $V_{bias} = -0.2$ V. Computational parameters: $V = -0.1$ V; ILDOS isosurface lying at ≈2 Å above graphene and with ILDOS value of 5×10^{-5} $|e|/a_0^3$. Color coding of DFT relaxed structures: Ni atoms in the first, second, and third layers are rendered in light grey, grey, and dark grey, respectively; B atoms in green; graphene network in black.

Fig. S3. We tried to simulate several structures with one/few B atoms in and below the graphene network in order to understand the origin of these defects, providing a possible interpretation for two of them. Fig. S4 shows experimental as well as simulated images of the two most occurring defects of this kind, along with their respective ball-and-stick models in the optimized DFT structure.

The STM images presented so far are related to regions with a lower concentration of B atoms in the graphene network. We also found a few regions where the observed density of B atom defects is much higher. An example is shown in Fig. 4(a). Here, the most striking feature is the tendency of B-fcc defects to align along the (−110) crystallographic direction. Rectangular marked regions in Fig. 4(a) represent some of the most common arrangements of aligned B-fcc defects, as confirmed by comparison with simulated STM images (Fig. 4(b), (c), and (d) and ball-and-stick models in their optimized DFT structure corresponding to the defects marked in the image Fig. 4(a)).

It should be noted that, with an increasing number of contiguously aligned defects, the appearance of the dark triangular feature seems to get more intense and darker, indicating a prominent effect on the local density of states and suggesting these could be potential active sites, e.g. for catalysis and gas sensing. Previous theoretical calculations indicate that the B-doped topological line defect in graphene act as a sensing material for various gas molecules. These B-doped topological line defect are metallic in nature which further favors the adsorption of NO and NH_3 over CO and CO_2 molecules. The electronic transport calculations reveal that the electric current can be confined to the line defect region by gate voltage control, revealing highly reactive sites [26].

It has been previously observed that mainly the changes in the synthesis method, growth conditions, and post-growth treatment determines the presence of selective defects and their density on the surface, which in turn can tune the electronic properties of as-grown B-graphene layers. Here, we have observed such change in defect density (low as well as high concentration regions of B) on different regions of the samples grown under the same growth parameters. This suggests that B atoms are non-uniformly distributed in the subsurface of the Ni (111) single crystal. Previous theoretical calculations indicate that, at high coverage, B atoms prefer to occupy subsurface Oct sites rather than on-surface sites and that the B stability slightly increases with concentration [51]. In summary, previous computational studies suggest that subsurface B prefers to form clusters rather than distribute evenly [51].

Along with the signature defects, namely B-fcc and B-top, and the alignment of the B-fcc, two larger and brighter features are visible in Fig. 4(a) (encircled in yellow). Similar features were previously observed in pristine graphene and assigned to Ni adatoms trapped in the graphene network during the growth process [53,57,58]. The active participation of such Ni adatoms in the process of graphene formation has been extensively demonstrated both experimentally and theoretically. They act as a catalyzing agent in the C–C bond formation during the CVD growth process and hence sometimes they remain trapped in the graphene network [36,57]. We also mention that C vacancies are rarely observed in CVD graphene on Ni(111), as proved in a previous combined experimental and theoretical work of some of us [58].

It has been previously reported that, for higher B concentration, B-graphene on Ni(111) and Co(0001) single crystals is not well-ordered, consisting of many misoriented domains separated by defective grain boundaries [30]. Conversely, in the present case, even in the higher concentration regions the honeycomb lattice does not appear to be distorted, indicating that our growth method, with the B segregation in

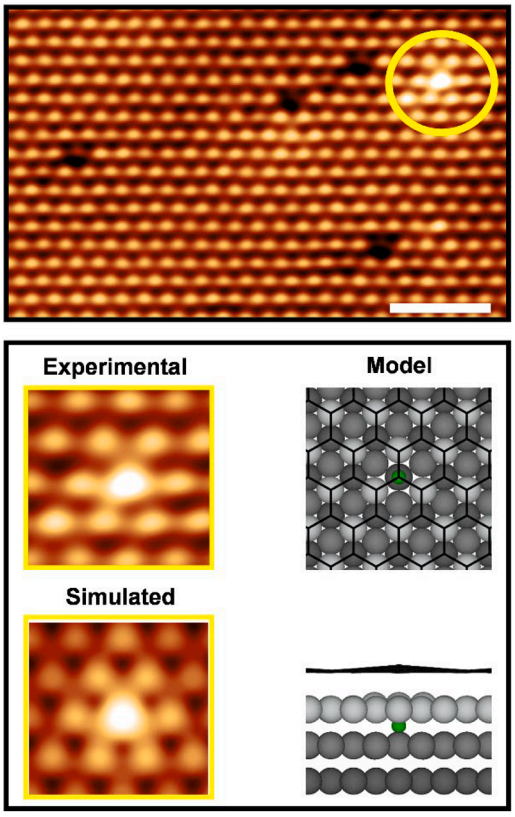

Fig. 3. STM image showing B at the Oct site in the subsurface. In the inset, the STM simulation along with the ball-and-stick model is visualized. Scale bar 1.5 nm. Experimental parameters: $I = 3.0$ nA, $V_{bias} = -0.2$ V. Computational parameters: $V = -0.1$ V; ILDOS isosurface lying ≈2 Å above graphene and with ILDOS value of 5×10^{-5} $|e|/a_0^3$. Color coding: Ni atoms in the first, second, and third layers are rendered in light grey, grey, and dark grey, respectively; B atoms in green; graphene network in black.

the bulk of Ni(111) single crystal, allows incorporation of B atoms in the graphene network at higher concentration without affecting the quality of the layer, which was not possible to achieve so far.

Finally, Fig. 4(a) also indicates that, when B atoms are present in higher concentrations in the B-graphene network, the occupancy of the fcc site is dominant over the top site, resulting in asymmetric sublattice doping. Theory suggests that asymmetric doping could be a promising way to generate a reproducible intrinsic band gap in doped graphene, especially in the case of N-doped and B-doped graphene [59–61] while, when the substitutional dopants are randomly distributed in the two sublattices, the resulting graphene-based material remains gapless [62]. Experimental observation of such unbalanced sublattice doping is still quite rare [59] an asymmetry doping was detected with STM in N-doped graphene, grown on a Cu(111) substrate [63], whereas measurements performed on B-graphene on Cu(111) revealed no doping asymmetry [29]. Recently, asymmetric B doping was observed in graphene grown on Ir(111) by STM measurements and confirmed by DFT calculations [64].

In order to further understand the effect of this asymmetric doping in B-graphene, we considered three isomers formed by choosing different doping sites for the same concentration of B atoms. Fig. S5 shows the optimized geometries of these three free-standing B-doped structures along with their computed band structures. Notably, despite all B atoms occupying a single sublattice (as shown in the middle and right panels of Fig. S5), the distribution across the graphene lattice significantly influences the degree of band gap opening. Particularly striking is the observation that maximal band gap occurs when all dopants are aligned, as a consequence of both sublattice symmetry breaking and the level of alignment achieved. To further validate this point, we considered three different B concentrations (from 2.78 % to 5.55 %), where, even though B atoms are present in the same sublattice, there are two distinct arrangements (random and line). Figure S6 shows these optimized free-standing B-doped structures. Interestingly, looking at the calculated band structure (Fig. S7), we observed how the B alignment (Fig. S6, line) allows for a larger band gap opening as compared to the equally spaced configurations (Fig. S6, random), keeping the same B concentration. Hence one can expect that the extent of band gap opening can be tuned not only by restricting B atoms in one of the sublattice, but also by controlling the extent of their alignment. Finally, to assess the stability of B-graphene structures (refer to Figure S6), we determined both the lattice cohesive and B dopant formation energies (as shown in Table S1), following the methodologies detailed in Ref. [65] and [23] respectively. Formation energies for both single and multiple B dopants in graphene

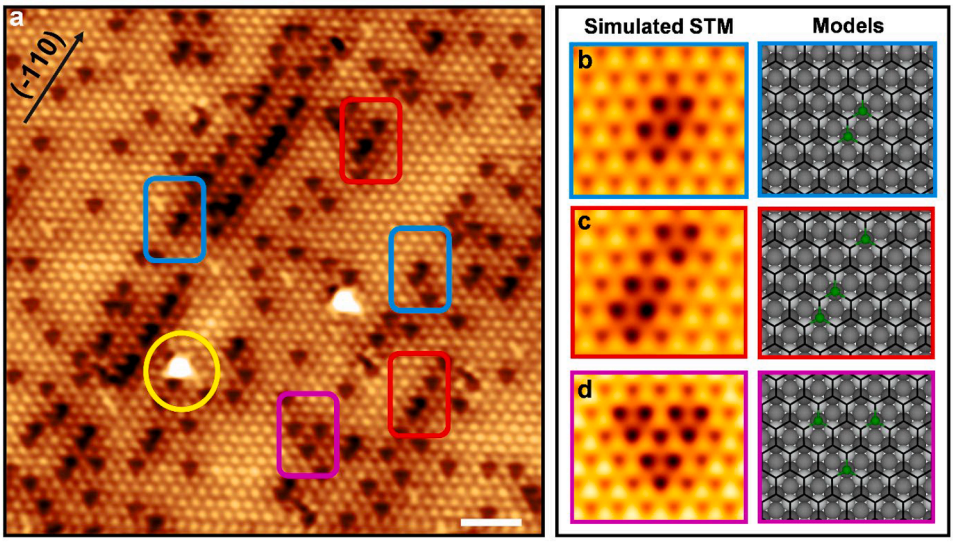

Fig. 4. (a) STM image depicting the presence of both signature defects (B-fcc, B-top) in B-graphene along with the alignment of B-fcc defects. Right panels (b, c, and d) show the simulated images, along with optimized ball-and-stick models, of the most observed alignments which are marked in the experimental STM image. Scale bar 1.5 nm. Experimental parameters: $I = 3.0$ nA, $V_{bias} = -0.2$ V. Computational parameters: $V = -0.1$ V; ILDOS isosurface lying ≈2 Å above graphene and with ILDOS value of 5×10^{-5} $|e|/a_0^3$.

fall within the range of 1.2 to 1.5 eV, aligning well with previous theoretical findings for similar concentrations [23].

We have observed two distinct regions with respect to B concentration in the as-grown graphene network, out of which the higher B concentration region, especially with the alignment of B-fcc defects, seems to exhibit a strong localized effect on the electronic properties. Further studies and optimization of growth parameters to maximize the coverage of these regions, as well as the alignment of B-fcc defects, would be therefore desirable to improve control over tuning the chemistry of graphene.

4. Conclusion

A novel, contamination-free, and versatile method for synthesizing selectively B-doped graphene on Ni(111) single crystal is proposed, based on the incorporation - during standard CVD growth - of B atoms segregating from a reservoir deliberately created in the substrate. This highly reproducible method of growing B-graphene leads to the formation of high-quality flat layers with several B defects embedded in the network. A thorough STM and XPS characterization, complemented by DFT calculations and STM simulations, allowed us to identify B atoms in the fcc sites of the graphene layer, as well as, for the first time, in the top sites. In addition, we demonstrate the presence of B atoms in the subsurface of Ni, specifically in octahedral configuration, further validating our method. Extensive high-resolution STM investigations showed the co-existence of low as well as high B-doping concentration regions in the graphene layer, probably stemming from the non-uniform presence of B in the Ni(111) bulk. Remarkably, in the high B concentration regions, B defects tend to align along specific crystallographic directions and show a strong preference to occupy one of the graphene sublattices. This results in asymmetric sublattice doping, which is predicted to generate an intrinsic band gap in graphene. The designed method for the incorporation of B atoms in graphene could be a substantial step forward in understanding or producing asymmetric sublattice doping, fostering its application in next-generation electronic devices. Furthermore, the aligned B defects can possibly serve as potential active sites, e.g. for catalysis and gas sensing.

CRediT authorship contribution statement

Sumati Patil: Writing – original draft, Visualization, Validation, Methodology, Investigation, Formal analysis, Data curation, Conceptualization. **Daniele Perilli:** Writing – review & editing, Visualization, Validation, Software, Investigation, Formal analysis. **Mirco Panighel:** Writing – review & editing, Validation, Investigation, Formal analysis, Data curation. **Anu Baby:** Software, Investigation, Formal analysis. **Cinzia Cepek:** Writing – review & editing, Visualization, Investigation, Formal analysis, Conceptualization. **Giovanni Comelli:** Writing – review & editing, Supervision, Conceptualization. **Cristiana Di Valentin:** Writing – review & editing, Supervision, Software, Project administration, Funding acquisition, Conceptualization. **Cristina Africh:** Writing – review & editing, Supervision, Resources, Project administration, Funding acquisition, Conceptualization.

Declaration of competing interest

The authors declare that they have no known competing financial interests or personal relationships that could have appeared to influence the work reported in this paper

Data availability

All data needed to evaluate the conclusions in the paper are available at https://doi.org/10.5281/zenodo.10419283, https://doi.org/10.5281/zenodo.1041928.

Acknowledgements

We acknowledge support from the Italian Ministry of Education, Universities and Research (MIUR) through the program PRIN 2017 - Project no. 2017NYPHN8. S.P. acknowledges support by the 'ICTP TRIL Programme, Trieste, Italy' in the framework of the agreement with CNR-IOM laboratories. M.P. acknowledges funding from the European Union's Horizon 2020 research and innovation programme under grant agreement No 101007417 NFFA-Europe Pilot. We thank Ayesha Farooq for her help with XPS experiments. D.P. and C.D.V acknowledge funding from the European Union – NextGenerationEU through the Italian Ministry of University and Research under PNRR – M4C2I1.4 ICSC – Centro Nazionale di Ricerca in High Performance Computing, Big Data and Quantum Computing (Grant No. CN00000013 and Innovation Grant with Leonardo and Ferrovie dello Stato).

Supplementary materials

Supplementary material associated with this article can be found, in the online version, at doi:10.1016/j.surfin.2024.104700.

References

[1] K.S. Novoselov, A.K. Geim, S.V. Morozov, D. Jiang, Y. Zhang, S.V. Dubonos, I. V. Grigorieva, A.A. Firsov, Electric field effect in atomically thin carbon films, Science 306 (5696) (2004) 666–669. https://www.science.org/doi/10.1126/science.1102896.

[2] K.S. Novoselov, A.K. Geim, S.V. Morozov, D. Jiang, M.I. Katsnelson, I. V. Grigorieva, S.V. Dubonos, A.A. Firsov, Two-dimensional gas of massless Dirac fermions in graphene, Nature 438 (7065) (2005) 197–200. https://www.nature.com/articles/nature04233.

[3] K.I. Bolotin, K.J. Sikes, Z. Jiang, M. Klima, G. Fudenberg, J. Hone, P. Kim, H. L. Stormer, Ultrahigh electron mobility in suspended graphene, Solid State Commun. 146 (2008) 351–355. https://www.sciencedirect.com/science/article/abs/pii/S0038109808001178.

[4] C. Lee, X. Wei, J.W. Kysar, J. Hone, Measurement of the elastic properties and intrinsic strength of monolayer graphene, Science 321 (5887) (2008) 385–388. https://www.science.org/doi/10.1126/science.1157996.

[5] A.K. Geim, K.S. Novoselov, The rise of graphene, Nat. Mater. 6 (3) (2007) 183–191. https://www.nature.com/articles/nmat1849.

[6] M.G. Betti, E. Placidi, C. Izzo, E. Blundo, A. Polimeni, M. Sbroscia, J. Avila, P. Dudin, K. Hu, Y. Ito, D. Prezzi, M. Bonacci, E. Molinari, C. Mariani, Gap opening in double-sided highly hydrogenated free-standing graphene, Nano Lett. 22 (7) (2022) 2971–2977. https://pubs.acs.org/doi/10.1021/acs.nanolett.2c00162.

[7] H.Y. Mao, Y.H. Lu, J.D. Lin, S. Zhong, A.T.S. Wee, W. Chen, Manipulating the electronic and chemical properties of graphene via molecular functionalization, Prog. Surf. Sci. 88 (2) (2013) 132–159. https://www.sciencedirect.com/science/article/abs/pii/S0079681613000038.

[8] L.S. Panchakarla, K.S. Subrahmanyam, S.K. Saha, A. Govindaraj, H. R. Krishnamurthy, U.V. Waghmare, C.N.R. Rao, Structure, and properties of boron- and nitrogen-doped graphene, Adv. Mater. 21 (46) (2009) 4726–4730, https://doi.org/10.1002/adma.200901285.

[9] D. Perilli, S. Fiori, M. Panighel, H. Liu, C. Cepek, M. Peressi, G. Comelli, C. Africh, C.D. Valentin, Mechanism of CO intercalation through the graphene/Ni(111) interface and effect of doping, J. Phys. Chem. Lett. 11 (20) (2020) 8887–8892. https://pubs.acs.org/doi/full/10.1021/acs.jpclett.0c02447.

[10] D. Wei, Y. Liu, Y. Wang, H. Zhang, L. Huang, G. Yu, Synthesis of N-doped graphene by chemical vapor deposition and its electrical properties, Nano Lett. 9 (5) (2009) 1752–1758. https://pubs.acs.org/doi/abs/10.1021/nl803279t.

[11] P. Błoński, J. Tuček, Z. Sofer, V. Mazánek, M. Petr, M. Pumera, M. Otyepka, R. Zbořil, Doping with graphitic nitrogen triggers ferromagnetism in graphene, J. Am. Chem. Soc. 139 (8) (2017) 3171–3180. https://pubs.acs.org/doi/10.1021/jacs.6b12934.

[12] W. Hu, C. Wang, H. Tan, H. Duan, G. Li, N. Li, Q. Ji, Y. Lu, Y. Wang, Z. Sun, F. Hu, W. Yan, Embedding atomic cobalt into graphene lattices to activate room-temperature ferromagnetism, Nat. Commun. 12 (1) (2021) 1854. https://www.nature.com/articles/s41467-021-22122-2.

[13] V.K. Paidi, E. Jung, J. Lee, A.T. Lee, M. Shepit, K. Ihm, B.H. Lee, J.V. Lierop, T. Hyeon, K.S. Lee, Robust room temperature ferromagnetism in cobalt doped graphene by precision control of metal ion hybridization, Adv. Funct. Mater. 33 (3) (2023) 2210722. https://onlinelibrary.wiley.com/doi/10.1002/adfm.202210722.

[14] X.K. Kong, C.L. Chen, Q.W. Chen, Doped graphene for metal-free catalysis, Chem. Soc. Rev. 43 (8) (2014) 2841–2857. https://pubs.rsc.org/en/content/articlelanding/2014/cs/c3cs60401b.

[15] Y. Jiao, Y. Zheng, M. Jaroniec, S.Z. Qiao, Origin of the electrocatalytic oxygen reduction activity of graphene-based catalysts: a roadmap to achieve the best performance, J. Am. Chem. Soc. 136 (11) (2014) 4394–4403. https://pubs.acs.org/doi/full/10.1021/ja500432h.

[16] L. Wang, Z. Sofer, M. Pumera, Will any crap we put into graphene increase its electrocatalytic effect? ACS Nano 14 (1) (2020) 21–25. https://pubs.acs.org/doi/10.1021/acsnano.9b00184.

[17] H. Wang, T. Maiyalagan, X. Wang, Review on recent progress in nitrogen-doped graphene: synthesis, characterization, and its potential applications, ACS Catal. 2 (5) (2012) 781–794. https://pubs.acs.org/doi/10.1021/cs200652y.

[18] C. Riedl, C. Coletti, U. Starke, Structural and electronic properties of epitaxial graphene on SiC(0 0 0 1): a review of growth, characterization, transfer doping and hydrogen intercalation, J. Phys. D Appl. Phys. 43 (37) (2010) 374009. https://iopscience.iop.org/article/10.1088/0022-3727/43/37/374009.

[19] L. Ferrighi, M.I. Trioni, C.D. Valentin, Boron-doped, nitrogen-doped, and codoped graphene on Cu(111): a DFT + vdW study, J. Phys. Chem. C 119 (11) (2015) 6056–6064. https://pubs.acs.org/doi/abs/10.1021/jp512522m.

[20] S. Freddi, D. Perilli, L. Vaghi, M. Monti, A. Papagni, C. Di Valentin, L. Sangaletti, Pushing down the limit of NH3 detection of graphene-based chemiresistive sensors through functionalization by thermally activated tetrazoles dimerization, ACS Nano 16 (7) (2022) 10456–10469.

[21] M. Srivastava, A. Srivastava, DFT analysis of nitrogen and boron doped graphene sheet as lead detector, Mater. Sci. Eng. B 269 (2021) 115165.

[22] B. Kwon, H. Bae, H. Lee, S. Kim, J. Hwang, H. Lim, W.H. Lee, Ultrasensitive N-channel graphene gas sensors by nondestructive molecular doping, ACS Nano 16 (2) (2022) 2176–2187.

[23] T. M Dieb, Z. Hou, K. Tsuda, Structure prediction of boron-doped graphene by machine learning, J. Chem. Phys. 148 (24) (2018).

[24] J. Gebhardt, R.J. Koch, W. Zhao, O. Höfert, K. Gotterbarm, S. Mammadov, C. Papp, A. Görling, H.-P. Steinrück, Th. Seyller, Growth and electronic structure of boron-doped graphene, Phys. Rev. B. 87 (2013) 155437. https://journals.aps.org/prb/abstract/10.1103/PhysRevB.87.155437.

[25] W.C. Yen, H. Medina, J.S. Huang, C.C. Lai, Y.C. Shih, S.M. Lin, J.G. Li, Z.M. Wang, Y.L. Chueh, Direct synthesis of graphene with tunable work function on insulators via in situ boron doping by nickel-assisted growth, J. Phys. Chem. C. 118 (43) (2014) 25089–25096. https://pubs.acs.org/doi/10.1021/jp508365h.

[26] B.K. Rao, T.L.G. Cabral, D.C. de Melo Rodrigues, F.A. de Souza, W.L. Scopel, R. G. Amorim, R. Pandey, Boron-doped graphene topological defects: unveiling high sensitivity to NO molecule for gas sensing applications, Phys. Chem. Chem. Phys. 26 (5) (2024) 4466–4473.

[27] L. Ferrighi, M. Datteo, C.D. Valentin, Boosting graphene reactivity with oxygen by boron doping: density functional theory modeling of the reaction path, J. Phys. Chem. C 118 (1) (2014) 223–230. https://pubs.acs.org/doi/abs/10.1021/jp410966r.

[28] G. Fazio, L. Ferrighi, C.D. Valentin, Boron-doped graphene as active electrocatalyst for oxygen reduction reaction at a fuel-cell cathode, J. Catal. 318 (2014) 203–210. https://www.sciencedirect.com/science/article/abs/pii/S0021951714002139.

[29] L. Zhao, M. Levendorf, S. Goncher, T. Schiros, L. Palová, A. Zabet-Khosousi, K. T. Rim, C. Gutíerrez, D. Nordlund, C. Jaye, M. Hybertsen, D. Reichman, G. W. Flynn, J. Park, A.N. Pasupathy, Local atomic and electronic structure of boron chemical doping in monolayer graphene, Nano Lett. 13 (10) (2013) 4659–4665. https://pubs.acs.org/doi/10.1021/nl401781d.

[30] D.Y. Usachov, A.V. Fedorov, A.E. Petukhov, O.Y. Vilkov, A.G. Rybkin, M. M. Otrokov, A. Arnau, E.V. Chulkov, L.V. Yashina, M. Farjam, V.K. Adamchuk, B. V. Senkovskiy, C. Laubschat, D.V. Vyalikh, Epitaxial B-graphene: large-scale growth and atomic structure, ACS Nano 9 (7) (2015) 7314–7322. https://pubs.acs.org/doi/abs/10.1021/acsnano.5b02322.

[31] M.G. Rybin, I.I. Kondrashov, A.S. Pozharov, V.C. Nguyen, N.M. Phan, E. D. Obraztsova, In situ control of CVD synthesis of graphene film on nickel foil, Phys. Status Solidi B 255 (1) (2018) 1700414. https://onlinelibrary.wiley.com/doi/abs/10.1002/pssb.201700414.

[32] L. Gao, J.R. Guest, N.P. Guisinger, Epitaxial graphene on Cu(111), Nano Lett. 10 (9) (2010) 3512–3516. https://pubs.acs.org/doi/10.1021/nl1016706.

[33] S. Marchini, S. Günther, J. Wintterlin, Scanning tunneling microscopy of graphene on Ru(0001), Phys. Rev. B. 76 (2007) 075429. https://journals.aps.org/prb/abstract/10.1103/PhysRevB.76.075429.

[34] J. Coraux, A.T. N'Diaye, C. Busse, T. Michely, Structural coherency of graphene on Ir(111), Nano Lett. 8 (2) (2008) 565–570. https://pubs.acs.org/doi/abs/10.1021/nl0728874.

[35] D. Nečas, P. Klapetek, Gwyddion: an open-source software for SPM data analysis, Cent. Eur. J. Phys. 10 (1) (2012) 181–188.

[36] L.L. Patera, C. Africh, R.S. Weatherup, R. Blume, S. Bhardwaj, C.C. Cudia, A. K. Gericke, R. Schloegl, G. Comelli, S. Hofmann, C. Cepek, In situ observations of the atomistic mechanisms of Ni catalyzed low temperature graphene growth, ACS Nano 7 (9) (2013) 7901–7912. https://pubs.acs.org/doi/abs/10.1021/nn402927q.

[37] P. Giannozzi, S. Baroni, N. Bonini, M. Calandra, R. Car, C. Cavazzoni, D. Ceresoli, G.L. Chiarotti, M. Cococcioni, I. Dabo, A. Dal Corso, S. Fabris, G. Fratesi, S. de Gironcoli, R. Gebauer, U. Gerstmann, C. Gougoussis, A. Kokalj, M. Lazzeri, L. Martin-Samos, N. Marzari, F. Mauri, R. Mazzarello, S. Paolini, A. Pasquarello, L. Paulatto, C. Sbraccia, S. Scandolo, G. Sclauzero, A.P. Seitsonen, A. Smogunov, P. Umari, R.M. Wentzcovitch, QUANTUM ESPRESSO: a modular and open-source software project for quantum simulations of materials, J. Phys. Condens. Matter 21 (2009) 395502. https://iopscience.iop.org/article/10.1088/0953-8984/21/39/395502.

[38] P. Giannozzi, O. Andreussi, T. Brumme, O. Bunau, M. Buongiorno Nardelli, M. Calandra, R. Car, C. Cavazzoni, D. Ceresoli, M. Cococcioni, N. Colonna, I. Carnimeo, A. Dal Corso, S. de Gironcoli, P. Delugas, R.A. DiStasio Jr, A. Ferretti, A. Floris, G. Fratesi, G. Fugallo, R. Gebauer, U. Gerstmann, F. Giustino, T. Gorni, J. Jia, M. Kawamura, H.-Y. Ko, A. Kokalj, E. Küçükbenli, M. Lazzeri, M. Marsili, N. Marzari, F. Mauri, N.L. Nguyen, H.-V. Nguyen, A. Otero-de-la-Roza, L. Paulatto, S. Poncé, D. Rocca, R. Sabatini, B. Santra, M. Schlipf, A.P. Seitsonen, A. Smogunov, I. Timrov, T. Thonhauser, P. Umari, N. Vast, X. Wu, S. Baroni, Advanced capabilities for materials modelling with Quantum ESPRESSO, J. Phys. Condens. Matter 29 (2017) 465901. https://iopscience.iop.org/article/10.1088/1361-648X/aa8f79/meta.

[39] D. Vanderbilt, Soft self-consistent pseudopotentials in a generalized eigenvalue formalism, Phys. Rev. B. 41 (11) (1990) 7892–7895. https://journals.aps.org/prb/abstract/10.1103/PhysRevB.41.7892.

[40] K. Lee, É.D. Murray, L. Kong, B.I. Lundqvist, D.C. Langreth, Higher-accuracy van der Waals density functional, Phys. Rev. B. 82 (8) (2010) 081101. https://journals.aps.org/prb/abstract/10.1103/PhysRevB.82.081101.

[41] I. Hamada, M. Otani, Comparative van der Waals density-functional study of graphene on metal surfaces, Phys. Rev. B. 82 (15) (2010) 153412. https://journals.aps.org/prb/abstract/10.1103/PhysRevB.82.153412.

[42] V.R. Cooper, Van der Waals density functional: an appropriate exchange functional, Phys. Rev. B 81 (16) (2010) 161104.

[43] H. Muñoz-Galán, F. Vines, J. Gebhardt, A. Görling, F. Illas, The contact of graphene with Ni (111) surface: description by modern dispersive forces approaches, Theor. Chem. Acc. 135 (2016) 1–9.

[44] A. Garcia-Lekue, M. Ollé, D. Sánchez-Portal, J.J. Palacios, A. Mugarza, G. Ceballos, P. Gambardella, Substrate-induced stabilization and reconstruction of zigzag edges in graphene nanoislands on Ni (111), J. Phys. Chem. C 119 (8) (2015) 4072–4078.

[45] D.E. Parreiras, E.A. Soares, G.J.P. Abreu, T.E.P. Bueno, W.P. Fernandes, V.E. De Carvalho, R. Paniago, Graphene/Ni (111) surface structure probed by low-energy electron diffraction, photoelectron diffraction, and first-principles calculations, Phys. Rev. B 90 (15) (2014) 155454.

[46] E. Voloshina, Y. Dedkov, Graphene on metallic surfaces: problems and perspectives, Phys. Chem. Chem. Phys. 14 (39) (2012) 13502–13514.

[47] S. Del Puppo, V. Carnevali, D. Perilli, F. Zarabara, A.L. Rizzini, G. Fornasier, M. Peressi, Tuning graphene doping by carbon monoxide intercalation at the Ni (111) interface, Carbon 176 (2021) 253–261.

[48] H.J. Monkhorst, J.D. Pack, Special points for Brillouin-zone integrations, Phys. Rev. B. 13 (12) (1976) 5188. https://journals.aps.org/prb/abstract/10.1103/PhysRevB.13.5188.

[49] J. Tersoff, D.R. Hamann, Theory of the scanning tunneling microscope, Phys. Rev. B. 31 (2) (1985) 805. https://journals.aps.org/prb/abstract/10.1103/PhysRevB.31.805.

[50] K. Momma amd F. Izumi, VESTA3 for three-dimensional visualization of crystal, volumetric and morphology data, J. Appl. Crystallogr. 44 (6) (2011) 1272–1276. https://onlinelibrary.wiley.com/doi/abs/10.1107/S0021889811038970.

[51] J. Xu, M. Saeys, First principles study of the effect of carbon and boron on the activity of a Ni catalyst, J. Phys. Chem. C. 113 (2009) 4099–4106. https://pubs.acs.org/doi/abs/10.1021/jp805579d.

[52] F. Joucken, Y. Tison, J. Lagoute, J. Dumont, D. Cabosart, B. Zheng, V. Repain, C. Chacon, Y. Girard, A.R.B. Méndez, S. Rousset, R. Sporken, J.C. Charlier, L. Henrard, Localized state and charge transfer in nitrogen-doped graphene, Phys. Rev. B Condens. Matter Mater. Phys. 85 (2012) 161408. https://journals.aps.org/prb/abstract/10.1103/PhysRevB.85.161408.

[53] S. Fiori, D. Perilli, M. Panighel, C. Cepek, A. Ugolotti, A. Sala, H. Liu, G. Comelli, C. D. Valentin, C. Africh, "Inside out" growth method for high-quality nitrogen-doped graphene, Carbon 171 (2021) 704–710. https://www.sciencedirect.com/science/article/abs/pii/S0008622320309155.

[54] L. Zhao, R. He, K.T. Rim, T. Schiros, K.S. Kim, H. Zhou, C. Gutiérrez, S. P. Chockalingam, C.J. Arguello, L. Pálová, D. Nordlund, M.S. Hybertsen, D. R. Reichman, T.F. Heinz, P. Kim, A. Pinczuk, G.W. Flynn, A.N. Pasupathy, Visualizing individual nitrogen dopants in monolayer graphene, Science 333 (2011) 999–1003. https://www.science.org/doi/10.1126/science.1208759.

[55] W. Wan, H. Li, H. Huang, S.L. Wong, L. Lv, Y. Gao, A.T.S. Wee, Bottom-up growth of epitaxial graphene on 6H-SiC(0001), ACS Nano 8 (2014) 970–976. https://pubs.acs.org/doi/abs/10.1021/nn800711v.

[56] Y. Jian, H. Jihua, F. Dongyu, C. Shuhai, Z. Xingke, First-principles investigation on the interaction of boron atom with nickel Part I: from surface adsorption to bulk diffusion, J. Alloys Compd. 663 (2016) 116–122. https://www.sciencedirect.com/science/article/abs/pii/S0925838815319290.

[57] L.L. Patera, F. Bianchini, C. Africh, C. Dri, G. Soldano, M.M. Mariscal, M. Peressi, G. Comelli, Real-time imaging of adatom-promoted graphene growth on nickel, Science 359 (6381) (2018) 1243–1246. https://www.science.org/doi/10.1126/science.aan8782.

[58] V. Carnevali, L.L. Patera, G. Prandini, M. Jugovac, S. Modesti, G. Comelli, M. Peressi, C. Africh, Doping of epitaxial graphene by direct incorporation of nickel adatoms, Nanoscale 11 (21) (2019) 10358–10364. https://pubs.rsc.org/en/content/articlelanding/2019/nr/c9nr01072f.

[59] J.A. Lawlor, M.S. Ferreira, Sublattice asymmetry of impurity doping in graphene: a review, Nanotechnol 5 (2014) 1210–1217. https://www.beilstein-journals.org/bjnano/articles/5/133.

[60] A. Lherbier, A.R. Botello-Méndez, J.C. Charlier, Electronic and transport properties of unbalanced sublattice N-doping in graphene, Nano Lett. 13 (2013) 1446–1450. https://pubs.acs.org/doi/10.1021/nl304351z.

[61] P. Rani, V.K. Jindal, Designing band gap of graphene by B and N dopant atoms, RSC Adv. 3 (2013) 802–812. https://pubs.rsc.org/en/content/articlelanding/2013/ra/c2ra22664b.

[62] D.Y. Usachov, A.V. Fedorov, O.Y. Vilkov, A.E. Petukhov, A.G. Rybkin, A. Ernst, M. M. Otrokov, E.V. Chulkov, I.I. Ogorodnikov, M.V. Kuznetsov, L.V. Yashina, E. Y. Kataev, A.V. Erofeevskaya, V.Y. Voroshnin, V.K. Adamchuk, C. Laubschat, D. V. Vyalikh, Large-scale sublattice asymmetry in pure and boron-doped graphene,

Nano Lett. 16 (7) (2016) 4535–4543. https://pubs.acs.org/doi/abs/10.1021/acs.nanolett.6b01795.

[63] A. Zabet-Khosousi, L. Zhao, L. Pálová, M.S. Hybertsen, D.R. Reichman, A. N. Pasupathy, G.W. Flynn, Segregation of sublattice domains in Nitrogen-doped graphene, J. Am. Chem. Soc. 136 (4) (2014) 1391–1397. https://pubs.acs.org/doi/10.1021/ja408463g.

[64] M.G. Cuxart, D. Perilli, S. Tömekce, J. Deyerling, F. Haag, M. Muntwiler, F. Allegretti, C.D. Valentin, W. Auwärter, Spatial segregation of substitutional B atoms in graphene patterned by the moiré superlattice on Ir(111), Carbon 201 (2023) 881–890. https://www.sciencedirect.com/science/article/abs/pii/S0008622322008193.

[65] A. Tiwari, J. Palepu, A. Choudhury, S. Bhattacharya, S. Kanungo, Theoretical analysis of the NH3, NO, and NO2 adsorption on boron-nitrogen and boron-phosphorous co-doped monolayer graphene-a comparative study, FlatChem 34 (2022) 100392.